ChemComm

COMMUNICATION

View Article Online
View Journal | View Issue

Cite this: *Chem. Commun.*, 2024, **60**, 3806

Received 13th February 2024,
Accepted 7th March 2024

DOI: 10.1039/d4cc00720d

rsc.li/chemcomm

Synthesis, structure and reactivity of iminoborane radicals†

Hanqiang Wang [ab]

The synthesis, characterization and reactivities of iminoborane radicals were reported. Both X-ray analysis and density functional theory calculations revealed that the unpaired electron delocalizes over the N(1)–C(1)–B(1)–N(2) moiety. Radical trap reactions showed that this radical species acts as a boron radical. These reactions also serve as methods for the synthesis of Lewis base-stabilized oxyl-terminated iminoboranes.

Iminoboranes are a class of compounds featuring multiple bonds between the boron and nitrogen, where an imino group is bonded to a boron atom. The synthesis and reactivity of the iminoboranes have attracted significant interest, primarily due to their potential applications in building boron–nitrogen fused aromatic compounds and their diverse reactivity with transition metals and unsaturated substrates.[1] Regarding the construction of classical iminoboranes (**I**), Paetzold's group developed an efficient method for their construction, which involved an elimination reaction of (trimethylsilylamino)boron halides under vacuum, leading to the formation of the first iminoboranes.[2] In subsequent experiments, a range of isolable diorganoiminoboranes were effectively synthesized and characterized through the utilization of bulky alkyl, aryl, amino, silyl and boryl substituents.[3] Additionally, the employment of strong σ-donating Lewis bases at the boron site has facilitated the isolation of room-temperature-stable Lewis base-supported iminoboranes (**II**), which can be considered as isoelectronic analogues of imines.[4–9] Based on Lewis base-stabilized iminoboranes, Bertrand and Stephan discovered the synthesis of cationic iminoboryl–CAAC adducts (**III**) through anion exchange.[10] To explore synthetic methods for the functionalized iminoboranes, Braunschweig's group established a pathway to B-metal substituted iminoborane reagents (**IV**) through the insertion of transition metals into B–Br bonds, followed by metathesis of TMSBr.[11] Wesemann and coworkers demonstrated that germyl substituted iminoboranes (**V**) were easily obtained by the reactions of germaborenes with organoazides.[12] More recently, the group of Kong developed an effective dehydrohalogenation/deprotonation route for synthesizing *N*-metal substituted iminoboranes (**VI**).[13] Despite the exploration of various iminoborane derivatives, the iminoborane radical species still remains elusive. In this study, we explore the synthesis of the iminoborane radical and reveal its behavior as a boron radical (Scheme 1).

Reduction of imino(chloro)borane–carbene **1** by 1 equivalent of KC_8 in toluene afforded NMR-silent red crystalline solid **2** after recrystallization from toluene in 64% yield (Scheme 2). The single crystal structure of **2** unambiguously confirms a nearly linear C(1)–B(1)–N(2)–Si(1) iminoborane structure with

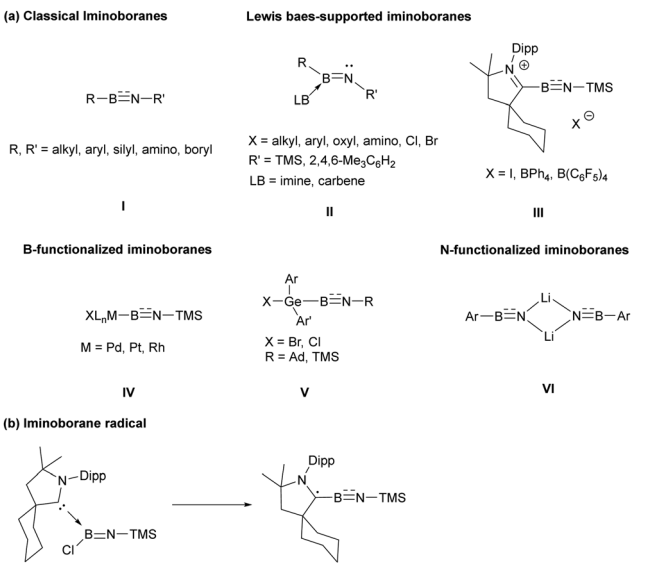

Scheme 1 Iminoborane derivatives.

[a] *Department of Chemistry and Dongguan Key Laboratory for Data Science and Intelligent Medicine, Great Bay University, Dongguan 523000, China. E-mail: hanqiangwang@gbu.edu.cn*
[b] *Department of Materials Science and Engineering, Southern University of Science and Technology (SUSTech), Shenzhen, Guangdong 518055, China*

† Electronic supplementary information (ESI) available. CCDC 2329996–2329998. For ESI and crystallographic data in CIF or other electronic format see DOI: https://doi.org/10.1039/d4cc00720d

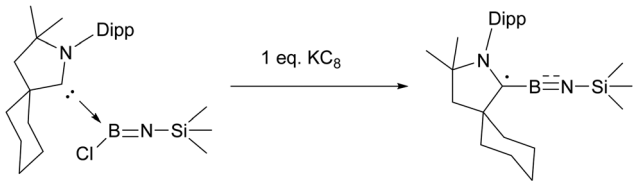

1 2

Scheme 2 Synthesis of carbene-stabilized iminoborane radicals.

the angles at B(1) (178.3(3)°) and N(2) (169.7(3)°), suggesting that the B(1) and N(2) atoms adopt sp hybridization (Fig. 1). The B(1)–N(2) (1.256(4) Å) distance in **2** falls in the range of typical BN triple bond distances (1.19–1.26 Å) in the reported iminoborane derivatives.[2–13] Most notably, the B(1)–C(1) distance (1.482(4) Å) is significantly shorter than the typical BC single bond (1.59 Å)[7] and carbene-supported neutral boron radicals (1.51–1.57 Å),[14] but is comparable to the BC double bond in the reported borataalkenes (1.44–1.53 Å).[15] Another noteworthy feature is that the C(1)–N(1) bond length of 1.374(3) Å falls in the range of typical C–N bond lengths (1.36–1.38 Å) in the reported structures.[14] These characteristics can be attributed to the substantial delocalization of the unpaired electron within the N(1)–C(1)–B(1)–N(2) unit.

To investigate more about unique the structural and electronic properties, the electronic structures and bonding properties of **2** were studied by density functional theory (DFT) calculations at the B3LYP level of theory (see the ESI† for detail). The plot of molecular orbitals shows that the SOMO is dominated by the contribution of the N–C π* and B=N π* orbitals (Fig. 2a), which is consistent with the shortened B–C bond and lengthened B–N/C–N bonds compared to the cationic iminoboryl–carbene species.[10]

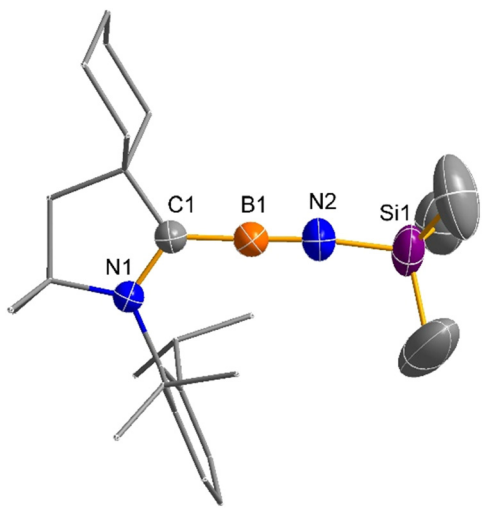

Fig. 1 Molecular structure of **2**. Thermal ellipsoids set at 50% probability. For clarity, carbene moieties are drawn in wireframe and hydrogen atoms are omitted. Selected bond [Å] and angles [°]: Si(1)–N(2) 1.675(3), B(1)–N(2) 1.256(4), B(1)–C(1) 1.482(4), N(1)–C(1) 1.374(3), N(2)–B(1)–C(1) 178.3(3), B(1)–N(2)–Si(1) 169.7(3), and N(1)–C(1)–B(1) 123.2(2).

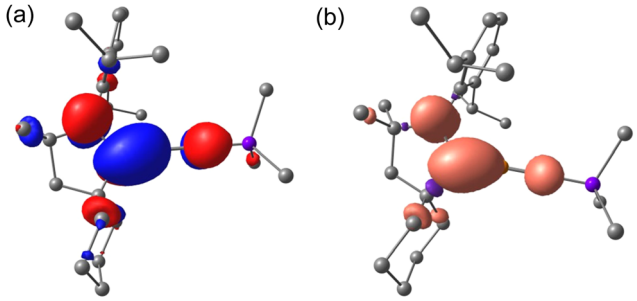

Fig. 2 SOMO (a) and spin population (b) plot of the optimized structure of **2** calculated at the B3LYP/6-31G+(d,p) level of theory.

Meanwhile, the B=N π-bonding can be seen from the HOMO−3 and HOMO−4 (See the ESI†). Natural bond orbital (NBO) analysis reveals one σ- and two π-bonding features of the BN unit with a significant contribution from the N atom, which is in line with the typical iminoborane derivatives. The Wiberg bond indexes (WBIs) of the C(1)–B(1), C(1)–N(1) and B(1)–N(2) bonds reach 1.10, 1.27 and 1.81, respectively, which proves the delocalization of unpaired electrons over the N(1)–C(1)–B(1)–N(2) moiety.

The radical **2** was further confirmed by EPR spectroscopy. EPR spectroscopy unambiguously confirmed the radical character of iminoborane **2**, which exhibits multiple-line spectra in toluene at room temperature centered at g_{iso} = 2.0015. Despite the intricacies of the hyperfine splitting, simulated spectra were successfully generated for **2** with hyperfine coupling constants of a($^{11,\ 10}$B) = 10.36/3.45 G, a($^{14}N_{CAAC}$) = 6.39 G, and a($^{14}N_{BN}$) = 1.62 G. The spin population plot of the optimized structure of **2** indicates that the unpaired spin density is mainly localized on C(1) (0.399), followed by N(1) (0.228), N(2) (0.100) and B(1) (0.077) (Fig. 2b). The low spin density on the B(1) atom is mainly attributed to π donation from lone electron pairs of the N(2) atom.[16]

The reactivity of compound **2** was explored through reactions with oxygen-containing radical trap reagents. Treatment of **2** with 0.5 equivalent of anthraquinone resulted in the formation of Lewis base-stabilized oxyl-terminated iminoborane **3** in a yield of 28% (Scheme 3). The ^{11}B NMR spectrum displayed a signal at 19.4 ppm, indicative of the boron atom binding to the oxygen atom. The solid-state structure of **3**, confirmed by single crystal X-ray analyses (Fig. 3), reveals a twisted O(1)–B(1)–N(2)–Si(1) skeleton, where two oxygen atoms from anthraquinone connect to two iminoborane molecules. The angles of N(2)–B(1)–O(1) and B(1)–N(2)–Si(1) are determined to be 131.3(4)° and 160.0(3)°, respectively. Notably, the B(1)–N(2)–Si(1) angle is significantly wider compared to reported Lewis base-stabilized iminoboranes.[7,10] The B(1)–N(2) distance (1.319(5) Å) is comparable with the typical B–N double bond in the reported Lewis base-stabilized oxyl-terminated iminoboranes.[8] The trimethylsilyl groups are positioned at the bottom/top of the anthraquinone plane, in agreement with the proton NMR shift at −1.02 ppm, reflecting the aromatic shielding effect. In the same manner, Lewis base-stabilized iminoboranes **4** were easily obtained by reacting **2**

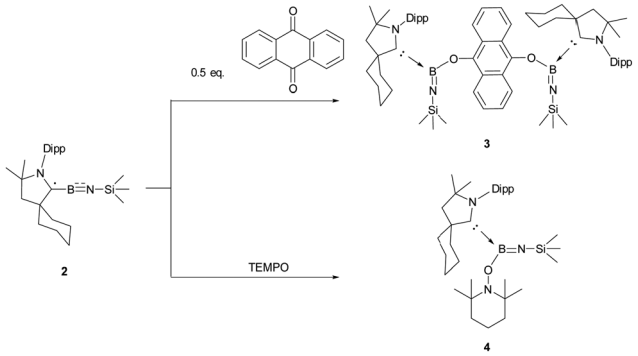

Scheme 3 Synthesis of **3 and 4**.

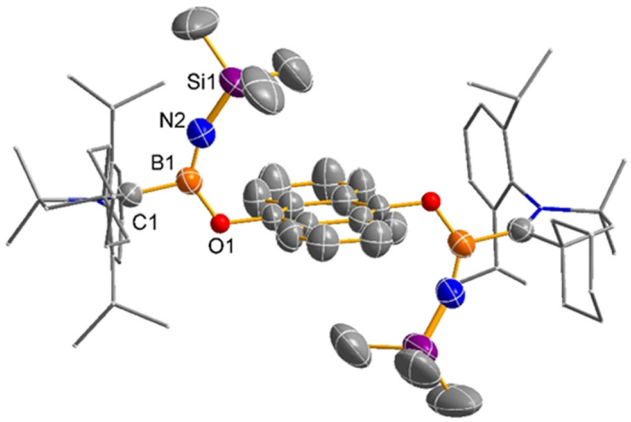

Fig. 3 Molecular structure of **3**. Thermal ellipsoids set at 50% probability. For clarity, the carbene moieties are drawn in wireframe and hydrogen atoms are omitted. Selected bond lengths [Å] and angles [°]: Si(1)–N(2) 1.655(4), O(1)–B(1) 1.409(5), B(1)–N(2) 1.319(5), B(1)–C(1) 1.590(6), N(1)–C(1) 1.301(4), N(2)–B(1)–O(1) 131.3(4), N(2)–B(1)–C(1) 114.6(4), O(1)–B(1)–C(1) 114.0(3), and B(1)–N(2)–Si(1) 160.0(3).

with 1 equivalent of 2,2,6,6-tetramethylpiperidinooxy in an 81% yield (Scheme 3). The ^{11}B NMR spectrum exhibits a signal at 19.4 ppm, indicating a sp^2-hybridized boron atom. The solid-state structure of **4**, confirmed by single crystal X-ray analyses (Fig. 4), further supported its formation through this reaction pathway.

In summary, the synthesis, characterization and reactivity of radical iminoborane **2** have been reported. The EPR spectrum shows that the unpaired electron delocalizes over the N(1)–C(1)–B(1)–N(2) moiety. Radical **2** acts as a boron radical in these radical trap reactions. These works expanded on the diverse reactivity patterns of iminoborane radicals and enriched the iminoborane chemistry.

Financial support from the National Natural Science Foundation of China (No. 22301030), the Dongguan Science and Technology of Social Development Program (No. 20231800940612) and Great Bay University is gratefully acknowledged. This work was also supported by the Center for Computational Science and Engineering at Southern University of Science and Technology and Prof. Xugang Guo is acknowledged.

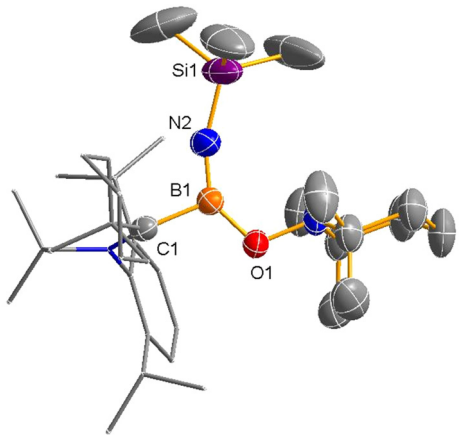

Fig. 4 Molecular structure of **4**. Thermal ellipsoids set at 50% probability. For clarity, the carbene moieties are drawn in wireframe and hydrogen atoms are omitted. Selected bond lengths [Å] and angles [°]: N(1)–C(16) 1.304 (2), B(1)–C(1) 1.621 (2), B(1)–N(2) 1.327(2), B(1)–O(1) 1.403(2), Si(1)–N(2) 1.658(2), N(2)–B(1)–O(1) 137.3 (2), N(3)–B(1)–C(16) 108.6(2), O(1)–B(1)–C(1) 114.1(2), and B(1)–N(2)–Si(1) 160.4(2).

Conflicts of interest

There are no conflicts to declare.

Notes and references

1 (*a*) B. Su and R. Kinjo, *Synthesis*, 2017, 2985–3034; (*b*) X. Chen, D. Tan and D. Yang, *J. Mater. Chem. C*, 2022, **10**, 13499–13532; (*c*) Y. Fan, J. Cui and L. Kong, *Eur. J. Org. Chem.*, 2022, e202201086; (*d*) L. Kong and C. Cui, *Synlett*, 2021, 1316–1322; (*e*) L. Winner, A. Hermann, G. Bélanger-Chabot, O. F. González-Belman, J. O. C. Jiménez-Halla, H. Kelchab and H. Braunschweig, *Chem. Commun.*, 2018, **54**, 8210–8213; (*f*) L. Winner, W. C. Ewing, K. Geetharani, T. Dellermann, B. Jouppi, T. Kupfer, M. Schäfer and H. Braunschweig, *Angew. Chem., Int. Ed.*, 2018, **57**, 12275–12279.
2 (*a*) H. Nöth, *Angew. Chem., Int. Ed. Engl.*, 1988, **27**, 1603–1623; (*b*) P. Paetzold, *Adv. Inorg. Chem.*, 1987, **31**, 123–170.
3 M. Bao, Y. Dai, C. Liu and Y. Su, *Inorg. Chem.*, 2022, **61**, 11137–11142.
4 L. Xie, J. Zhang, H. Hu and C. Cui, *Organometallics*, 2013, **32**, 6875–6878.
5 L. Xie, J. Zhang and C. Cui, *Chem. – Eur. J.*, 2014, **20**, 1–5.
6 H. Braunschweig, W. C. Ewing, K. Geetharani and M. Schafer, *Angew. Chem., Int. Ed.*, 2015, **54**, 1662–1665.
7 F. Dahcheh, D. Martin, D. W. Stephan and G. Bertrand, *Angew. Chem., Int. Ed.*, 2014, **53**, 13159–13163.
8 P. Cui, R. Guo, L. Kong and C. Cui, *Inorg. Chem.*, 2020, **59**, 5261–5265.
9 R. Guo, X. Zhang, T. Li, Q. Li, D. A. Ruiz, L. L. Liu, C. H. Tung and L. Kong, *Chem. Sci.*, 2022, **13**, 2303–2309.
10 F. Dahcheh, D. W. Stephan and G. Bertrand, *Chem. – Eur. J.*, 2015, **21**, 199–204.
11 (*a*) H. Braunschweig, K. Radacki, D. Rais and K. Uttinger, *Angew. Chem., Int. Ed.*, 2005, **45**, 162–165; (*b*) H. Braunschweig, T. Kupfer, K. Radacki, A. Schneider, F. Seeler, K. Uttinger and H. Wu, *J. Am. Chem. Soc.*, 2008, **130**, 7974–7983.
12 D. Raiser, H. Schubert, H. F. Bettinger and L. Wesemann, *Chem. – Eur. J.*, 2021, **27**, 1981–1983.
13 R. Guo, T. Li, R. Wei, X. Zhang, Q. Li, L. L. Liu, C. H. Tung and L. Kong, *J. Am. Chem. Soc.*, 2021, **143**, 13483–13488.
14 (*a*) P. Bissinger, H. Braunschweig, A. Damme, I. Krummenacher, A. K. Phukan, K. Radacki and S. Sugawara, *Angew. Chem., Int. Ed.*, 2014, **53**, 7360–7363; (*b*) A. D. Ledet and T. W. Hudnall, *Dalton Trans.*, 2016, **45**, 9820–9826; (*c*) W. Yang, K. E. Krantz, L. A. Freeman, D. A. Dickie, A. Molino, G. Frenking, S. Pan, D. J. D. Wilson and R. J. Gilliard Jr., *Angew. Chem., Int. Ed.*, 2020, **59**, 3850–3854;

(*d*) K. K. Hollister, W. Yang, R. Mondol, K. E. Wentz, A. Molino, A. Kaur, D. A. Dickie, G. Frenking, S. Pan, D. J. D. Wilson and R. J. Gilliard Jr, *Angew. Chem., Int. Ed.*, 2022, **61**, e202202516.

15 (*a*) J. Han, C. Hu, Q. Li, L. L. Liu, C. Tung, P. Cui and L. Kong, *Inorg. Chem.*, 2023, **62**, 18820–18824; (*b*) J. D. Hoefelmeyer, S. Solé and F. P. Gabbaï, *Dalton Trans.*, 2004, 1254–1258; (*c*) J. Mçbus, G. Kehr, C. G. Daniliuc, R. Frçhlich and G. Erker, *Dalton Trans.*, 2014, 632–638; (*d*) S. Kohrt, S. Dachwitz, C. G. Daniliuc, G. Kehra and G. Erker, *Dalton Trans.*, 2015, **44**, 21032–21040; (*e*) P. Moquist, G.-Q. Chen, C. Mück-Lichtenfeld, K. Bussmann, C. G. Daniliuc, G. Kehr and G. Erker, *Chem. Sci.*, 2015, **6**, 816–825.

16 (*a*) M.-A. Légaré, G. Bélanger-Chabot, R. D. Dewhurst, E. Welz, I. Krummenacher, B. Engels and H. Braunschweig, *Science*, 2018, **359**, 896–900; (*b*) Y.-J. Lin, W.-C. Liu, Y.-H. Liu, G.-H. Lee, S.-Y. Chien and C.-W. Chiu, *Nat. Commun.*, 2022, **13**, 7051; (*c*) Y. Aramaki, H. Omiya, M. Yamashita, K. Nakabayashi, S.-I. Ohkoshi and K. Nozaki, *J. Am. Chem. Soc.*, 2012, **134**, 19989–19992.